Journal of Materials Chemistry A
Supplementary Information

Surface functionalization of high free-volume polymers as a route to efficient hydrogen separation membranes

Behnam Ghalei,[a] Yosuke Kinoshita,[ab] Kazuki Wakimoto,[ab] Kento Sakurai,[ab] Simon Mathew,[c] Youfeng Yue,[d] Hiromu Kusuda,[b] Hiroshi Imahori [ae] and Easan Sivaniah[a]*

[a] *Institute for Integrated Cell-Material Sciences (iCeMS), Kyoto University, 606-8501 Kyoto, Japan. Email: esivaniah@icems.kyoto-u.ac.jp*
[b] *Graduate school of Energy Science, Kyoto University, 606-8501 Kyoto, Japan.*
[c] *van 't Hoff Institute for Molecular Sciences, Universiteit van Amsterdam, Science Park 904, 1098 XH Amsterdam, The Netherlands.*
[d] *Electronics and Photonics Research Institute, National Institute of Advanced Industrial Science and Technology (AIST), Tsukuba 305-8565, Japan.*
[e] *Department of Molecular Engineering, Graduate School of Engineering, Kyoto University, 615-8510 Kyoto, Japan*

PIM-1/PDA and PIM/PANI composite membranes with different coating times

Experimental methods

PIM-1 synthesis. The PIM-1 polymer was prepared according to the reported method by Budd *et al.* .[1] The polymer was synthesized from polycondensation reaction between 5,5',6,6'-tetrahydroxy-3,3,3',3'-tetramethyl-1,1'-spirobisindane (TTSBI, 30 mmol, Wako Pure Chemical) and 2,3,5,6-tetrafluoroterephthalonitrile (TFTPN, 30 mmol, Wako Pure Chemical) in the presence of dried K_2CO_3 (60 mmol, Sigma-Aldrich) and anhydrous dimethylformamide (DMF, 200 mL, Sigma-Aldrich) (Fig. S1). The reaction mixture was stirred under nitrogen atmosphere at 65 °C for 60 h. Then, the polymer was purified by dissolving in chloroform and re-precipitation from methanol, filtered and dried in vacuum oven at 110°C overnight. The molecular weight of purified polymer was determined from gel permeation chromatography (GPC), giving an average molecular weight of M_n= 90,000 to 120,000 Da and a polydispersity (PDI) of 2.2 to 2.5.

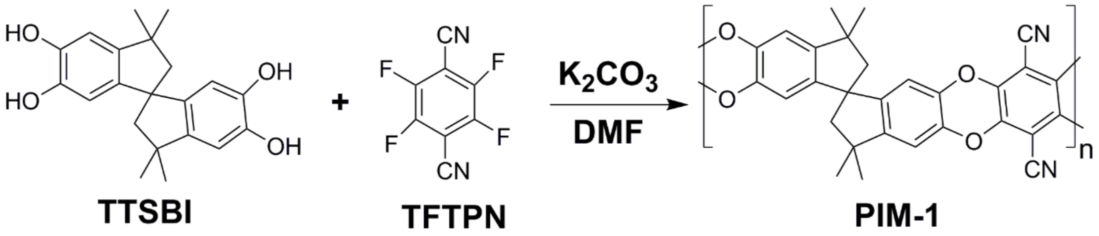

Fig. S1. Synthesis of PIM-1 and chemical structure.

PIM-1 and PTMSP membrane preparation. PIM-1 and PTMSP membranes were prepared by solution casting and solvent evaporation technique. Casting solutions were prepared from the dissolution of PIM-1 and PTMSP in chloroform and cyclohexane, respectively. The 8 wt. % polymer solutions were made by continuous stirring at room temperature and non-dissolved polymers were purified by filtration through PTFE filters or by centrifugation.

Polymer solution was cast on the glass substrate and covered in a clean chamber at room temperature under atmospheric pressure for slowly evaporation of the solvent. After 2 days, the resulting membrane was dried in a vacuum oven at 110 °C overnight.

Thickness of the membranes was around 80 µm as measured by a micrometer caliper. The average thickness of an individual membrane was measured based on the results of three separate thickness values at different points on the membrane surface.

Polydopamine synthesis. The dopamine solutions were prepared from dopamine hydrochloride (1, 2 and 4 mg mL^{-1}) in 10 mM Tris–HCl buffer (Fig. S2). The pH of Tris–HCl buffer solutions was adjusted to 7.5, 8.5 and 9.5 by 0.5 M NaOH solution prior to use. The prepared solution polymerized by air at different reaction times.

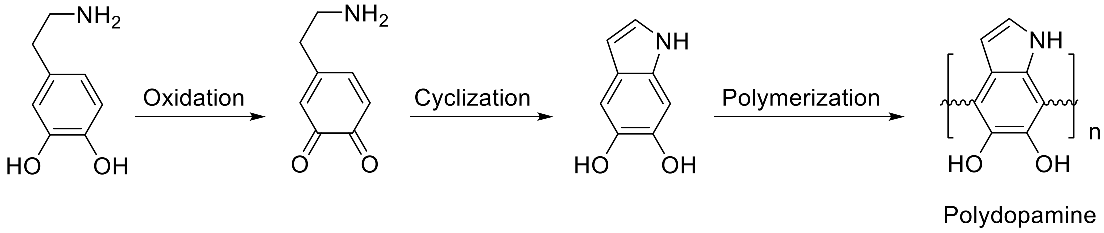

Fig. S2. Polydopamine synthesis and chemical structure.

Polyaniline synthesis. 0.596 g of aniline were added to 20 mL distilled water. The initial pH of the solution was adjusted to 3 by addition of 1 M HCl. 20 mL of ammonium peroxodisulfate (0.1 M) solution were added gradually to the reaction solution.

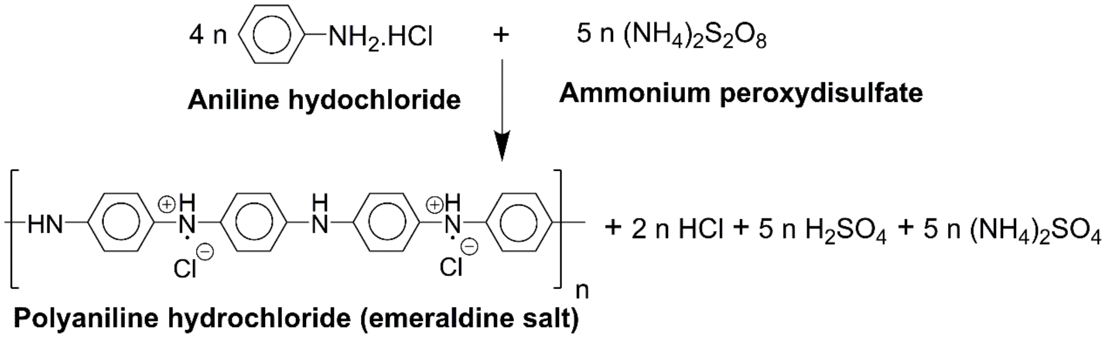

Fig. S3. Polyaniline synthesis and chemical structure.

Characterization methods

The obtained functional groups in synthesized PIM-1, PDA and PANI were investigated by the Fourier Transform Infrared spectrometer (FT-IR, Shimadzu, IRTracer-100), equipped with an attenuated total reflectance (ATR) cell in the range of 4000–500 cm^{-1}. All the films used for FT-IR measurement were prepared by casting the 1 wt. % polymer solutions on a KBr disc. The surface and cross-section morphology of the composite membranes were observed by an FESEM (Hitachi S-4800, Japan) instrument. Cross-sections of membranes were obtained by fracturing in liquid nitrogen and sputtered with osmium to prevent charging. The surface topography of samples also characterized using atomic force microscope (NanoWizard III, JPK Instruments, Japan) in tapping mode. X-ray photoelectron spectroscopy (XPS, ULVAC-PHI MT-5500) instrument using Mg Kα (1254.0 eV) as radiation source (the takeoff angle of the photoelectron was set at 90˚) was used to determine the composition of PDA and PANI on PIM-1 surface. Survey spectra were collected over a range of 0-1100 eV, and high-resolution spectra of C1s peak were also collected. The hydrophilicity of the film surface was characterized on the basis of static contact angle measurement using a contact angle goniometer (JC2000C, Japan) equipped with video capture. A piece of 2 cm^2 film was stick on a glass slide and mounted on the goniometer. A total of 10 µL droplet was dropped on the air side the membranes with a micropipette at room temperature. Nanoindentation was performed on the surface of pure PIM-1 and composite membranes using nanoindentation tester (ENT 2100, Elionix) equipped with a Berkovich three-sided pyramid diamond tip (radius of 100 nm) with the load range of 0.01 to 50 mN. Each indent was made in the samples up to a maximum depth of around 1 µm. 20 points in a rectangular configuration were tested on each sample; the average elastic modulus and hardness calculated based on the measured values of three different samples and derived by Oliver and Pharr's method.[2]

Gas permeation measurement. Pure gas permeabilities of the membranes were determined using the constant pressure-variable volume method at room temperature (25 ˚C). The membrane was held in a Millipore commercial filter holder with steel meshed supports, and rubber O-rings were used for proper sealing. The membrane evacuated with a vacuum pump (Edwards RV8) prior to gas permeation measurements. The gas permeate pressure were continuously recorded by pressure transmitters (Keller PAA 33X) connected to a data acquisition system. The slope of pressure increase (*dp*/*dt*) in the permeate chamber became constant at the pseudo-steady state. The gas permeability (*P*) is calculated based on the following equation:

$$P = \frac{Vl}{A}\frac{T_0}{p_f p_0 T}\left(\frac{dp}{dt}\right) \tag{1}$$

where *P* is the permeability of the gas through the membrane, in Barrer (1 Barrer=10^{-10} cm^3(STP)cm·cm^{-2}·s^{-1}·cmHg^{-1}), *V* is the permeate volume (cm^3), *l* is the thickness of membrane (cm), *A* is the effective area of the membrane (cm^2), p_f is the feed pressure (cmHg), p_0 is the pressure at standard state (76 cm-Hg), *T* is the absolute operating temperature (K), T_0 is the temperature at standard state (273.15 K), (*dp/dt*) is the slope of pressure increase in the permeate volume at pseudo-steady state (cmHg s^{-1}).

The diffusion coefficient (*D*) for a specific gas can be derived from the thickness of the membrane (*l*) and the time lag (ϑ):

$$D = \frac{l^2}{\vartheta} \tag{2}$$

Then the solubility (S) can be derived from:

$$S = \frac{P}{D} \tag{3}$$

The ideal selectivity ($\alpha_{\mathrm{A/B}}$) of gas pairs, A and B, is defined as:

$$\alpha_{\mathrm{A/B}} = \frac{P_{\mathrm{A}}}{P_{\mathrm{B}}} = \left[\frac{D_{\mathrm{A}}}{D_{\mathrm{B}}}\right]\left[\frac{S_{\mathrm{A}}}{S_{\mathrm{B}}}\right] \tag{4}$$

where D_A/D_B is the diffusivity selectivity and S_A/S_B is the solubility selectivity.

The feed side pressure of the gases ranged from 2 to 8 bar. Permeability coefficients were calculated three times for each membrane. The error for the absolute values of the permeability coefficients could be estimated to about ±7%, due to uncertainties in determination of the gas flux and membrane thickness. However, the reproducibility was better than ± 5%.

The membrane was exposed to CO_2/H_2 (50/50 vol. %, Kyoto Teisan Co.) mixed gas with feed pressure up to 8 bar at room temperature (25 °C), the feed flow rate was controlled by a metering valve and measured by a flow meter (Shimadzu, Japan). The stage cut, the ratio of permeate to feed flow rate, was less than 1% to keep composition similar in residue and feed. The mixed gas permeation and composition were measured using an in-line gas chromatograph (Shimadzu, model 2014) equipped with a thermal conductivity detector (TCD) in presence of controlled-flow argon as a carrier gas. By measuring the permeate flow rate (Q_P) and gas compositions with GC, the permeability of individual gases (*i)* through the membrane, P_i (Barrer) is calculated as:

$$P_i = \frac{Q_P x_{p,i} l}{A(p_f x_{f,i} - p_p x_{p,i})} \tag{5}$$

Where $x_{p,i}$ is the volume fraction of component *i* in the permeate gas; $x_{f,i}$ is the volume fraction of species *i* in the feed gas; *A* is the effective area of membrane (cm^2); *l* is the thickness of membrane (cm); p_f is the feed pressure (cmHg); p_p is the permeate pressure (cmHg). The selectivity is calculated from the ratio of gases permeabilites.

XPS analysis. Chemical composition of the membrane surface was determined by XPS (Fig. S4 (a) and (b)). The common view for dopamine polymerization is oxidation of the catechol to quinone form and cross-linking by the reverse reaction between catechol and o-quinone structure of dopamine molecules.[3] The adhesiveness of PDA is due to a combination of interactions from amino, imino, hydroxyl and catechol functional groups along with π-π interactions.[4] Deconvolution of the C1s core level spectrum revealed three peaks at 287.5, 285.5, and 284.5 eV, assigned to C=O, C-N/C-OH and C-H, respectively (see Fig. S4(c) and Fig. S5). The amount of C=O increased in dopamine solutions with higher pH, suggesting a higher pH promotes quinone functionality. The binding energy at 532.4 eV is assigned to oxygen from the catechol and quinine forms of dopamine (Fig. S4(a)). The surface elemental analysis of the PIM-1/PDA composite membranes revealed the N/C molar ratio increased and approached the theoretical value of pure dopamine (0.125) (see Table S1).

The XPS survey scan of PANI samples shows the presence of oxygen (O (1s) ~532 eV), nitrogen (N (1s) ~400 eV), carbon (C (1s) ~285 eV) and chlorine (Cl (2p) ~199 eV) (see Fig. S4(b)). The relative concentrations of the elements in the coated films, calculated from the corresponding photoelectron peak areas, are listed in Table S2. The small degree (5%) of oxygen content, in PANI films is suspected to originate from partial oxidation of the PANI surface.[5] The presence of carbon and nitrogen are ascribed to the PANI backbone, and the presence of chlorine is rationalized from its presence as a counter ion (in protonated PANI) or from traces of HCl employed in the polymerization solution. The oxygen content increased to 15% in the coated samples of poly (aniline-*co*-(*o*-methoxyaniline)), indicating successful incorporation of methoxy groups in the functionalized aniline monomer. In a similar fashion, the XPS for poly(aniline-*co*-(*m*-fluoroaniline) (1:1)) revealed F (1s) peak centered close to 697 eV confirming the presence of fluorine within the polymer on the surface of the coated sample.[6]

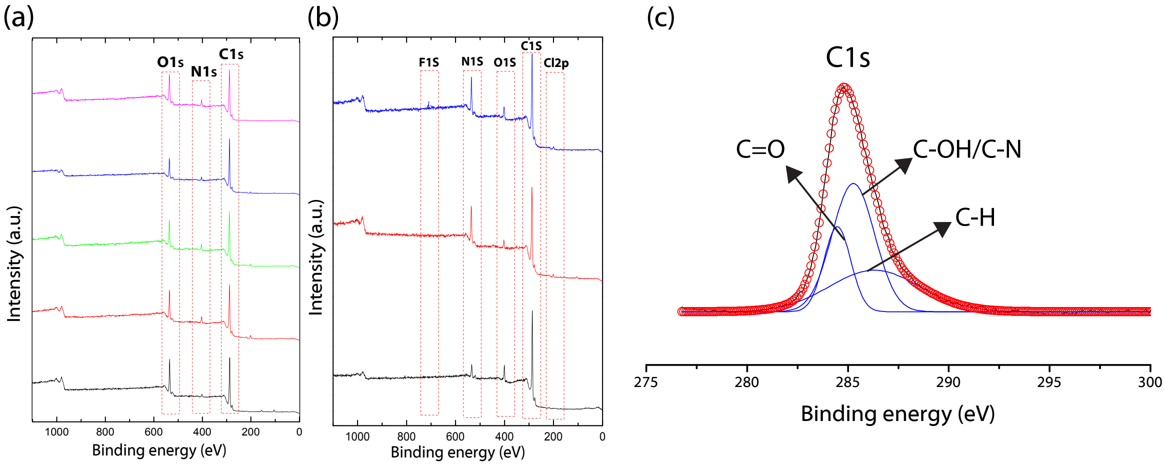

Fig. S4. (a) High resolution XPS spectra of PDA composite membranes after 120 min coating time: i) 2 mg mL^{-1}, pH 7.5 (black), ii) 2 mg mL^{-1}, pH 8.5 (red), iii) 2 mg mL^{-1}, pH 9.5 (green), iv) 4 mg mL^{-1}, pH 8.5 (blue), 1 mg mL^{-1}, pH 8.5 (pink). (b) High resolution XPS spectra of PANI composite samples after 24 min coating time, i) polyaniline (black), ii) poly(aniline-*co*-(*o*-methoxyaniline) (1:3, red), iii) poly(aniline-*co*-(*m*-fluoroaniline) (1:3, blue). (c) C1s spectra of PDA coated sample (2 mg mL^{-1}, pH 8.5, 120 min).

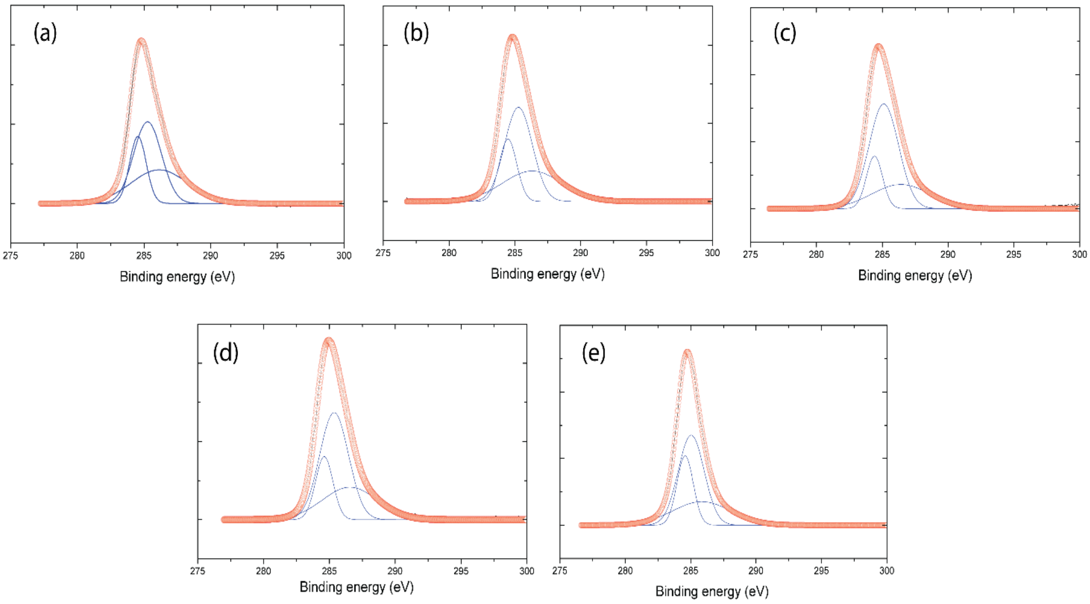

Fig S5. High resolution XPS spectra of polydopamine coated samples (120 min coating time) (a) dopamine concentration (1 mg mL^{-1}, pH 8.5) (b) dopamine concentration (2 mg mL^{-1}, pH 8.5) (c) dopamine concentration (4 mg mL^{-1}, pH 8.5) (d) dopamine concentration (2 mg mL^{-1}, pH 7.5) (e) dopamine concentration (1 mg mL^{-1}, pH 9.5).

Table S1. Surface elemental composition of the PIM-1 and PIM-1/PDA composite membranes with different pH and concentrations of the dopamine solution (coating time 120 min).

Sample (Concentration (mg mL^{-1}) - pH)	Surface elemental composition (mol. %)					
	C					
	C-H	C-N/C-OH	C=O	O	N	N/C
PIM-1	82			13	5	0.061
2 mg mL^{-1} - pH: 7.5	12.1	43.6	19.9	17	5.9	0.078
2 mg mL^{-1} - pH: 8.5	14.9	35.4	24.4	17.7	6.1	0.0817
2 mg mL^{-1} - pH: 9.5	15.9	32.7	27.3	18.7	5.4	0.0711
1 mg mL^{-1} - pH: 8.5	14.1	39.5	22.8	18.1	5.1	0.0668
4 mg mL^{-1} - pH: 8.5	19.1	39.3	23.2	14	3.8	0.046

Table S2. Surface elemental composition of the PIM-1 and PIM-1/PANI composite membranes (coating time 24 min).

Sample	Atom percentage (mol. %)							
	C							
	C-H	C-N/C=N	C=O	O	N	Cl	F	N/C
PIM-1	82			13	5	0	0	0.061
PIM-1/PANI	22.8	38.2	24.4	5.6	8.8	0.25	0	0.103
PIM-1/PANI-*co*-Poly(*o*-anisidine)	16.6	42.8	18.5	15.1	5.7	1.3	0	0.073
PIM-1/PANI-*co*-Poly(F-aniline)	13.3	53.7	13.1	10.1	7.8	0.8	1.2	0.097

FTIR of bulk PDA and PANI. The FTIR spectrum of the bulk PDA synthesized at different pH and concentrations is depicted in Fig. S6. The N-H and O-H stretching vibrations occur in a broad band at 3700–3000 cm^{-1}. Aliphatic C–H stretching mode is known to adsorb at about 2950-2850 cm^{-1}; and a broad peak centered at 1600 cm^{-1} is assigned to ν_{ring}(C=C) stretching vibrations. The PDA which is prepared in higher pH and concentration shows a band at 1710 cm^{-1} that is related to ν(C=O) groups, indicating the presence of quinone groups. For the samples prepared in lower pH and dopamine concentration, the 1710 cm^{-1} feature decreases in relative intensity, indicating that carbonyl species are a minor component of the bulk PDA film. pH value of the dopamine solution can control the equilibrium between catechol and quinone groups. At higher pH, catechol groups of dopamine are easily deprotonated and oxidized to quinone groups which subsequently effect on the microstructure, polarity and separation performance of PDA layer.[7] Two features at 1620 and 1510 cm^{-1} dispart from the broad band centered at around 1600 cm^{-1} and are assigned to ν_{ring}(C=C) and ν_{ring}(C=N) stretching modes, respectively, confirming the presence of aromatic amine species in the final PDA. The shoulder peak at 1350 cm^{-1}, is assigned to bicyclic ring CNC stretching modes. The presence of indole features in the bulk PDA supports the proposed structure of melanin-like polymers (*i.e.* polydopamine, dopamine-melanin) with 5,6-dihydroxyindole and/or 5,6-indolequinone units.[8]

Formation of polyaniline and its derivatives is also confirmed by FTIR. The FTIR spectrum of polyaniline (Fig. S7) has several major bands at 3450, 1580, 1450, 1290 and 1128 cm^{-1}.[9] The peak at 3450 cm^{-1} is attributed to N–H stretching modes, the peaks at around 1580 and 1450 cm^{-1} are attributed to C=N and C=C stretching modes for the quinoid and benzoic rings. The bands at about 1290 and 1250 cm^{-1} are related to C–N stretching of the benzenoid ring and the peak at 1135 and 810 cm^{-1} are assigned to the bending vibration of C–H, which is formed during protonation.[10] Poly(*o*-methoxyaniline) and its copolymers with aniline (Fig. 7(f)-(h)) showed bands at 1010 cm^{-1} assigned to C-O-C stretching of alkyl aryl ether linkage. Fig. 7(c)-(e) also present the FTIR bands observed for poly (*m*-fluoroaniline) and poly(aniline-*co*-(*m*-fluoroaniline)).[5] The absorption peak observed at 1170 cm^{-1} has been associated with the presence of a halogen (fluoro) group in the poly(*m*-fluoroaniline) and the copolymer. These vibration bands are also showed in the infrared spectrum of PANI (Fig. S7(a)). However, a shift observed in the spectrum indicates the presence of fluoro moieties in the polymer chain.[6]

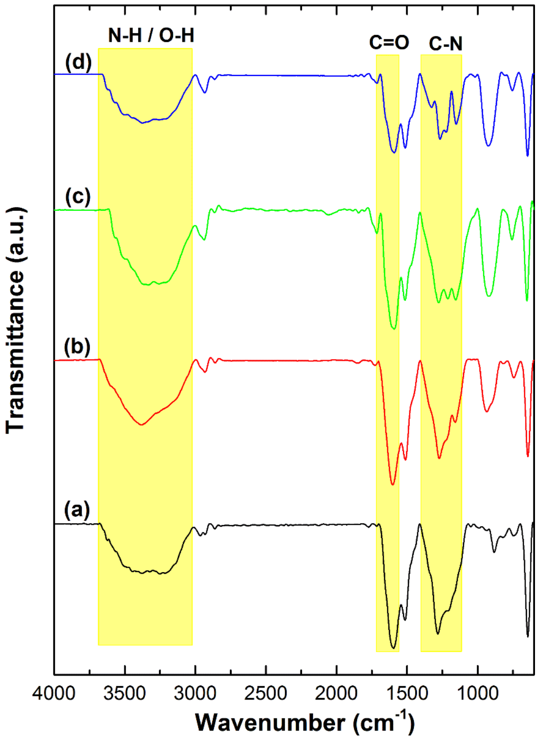

Fig. S6. FTIR of spectra of PDA in different dopamine concentrations and pH (a) 2 mg mL^{-1}, pH 7.5 (b) 2 mg mL^{-1}, pH: 8.5 (c) 2 mg mL^{-1}, pH 9.5 and (d) 4 mg mL^{-1}, pH 8.5.

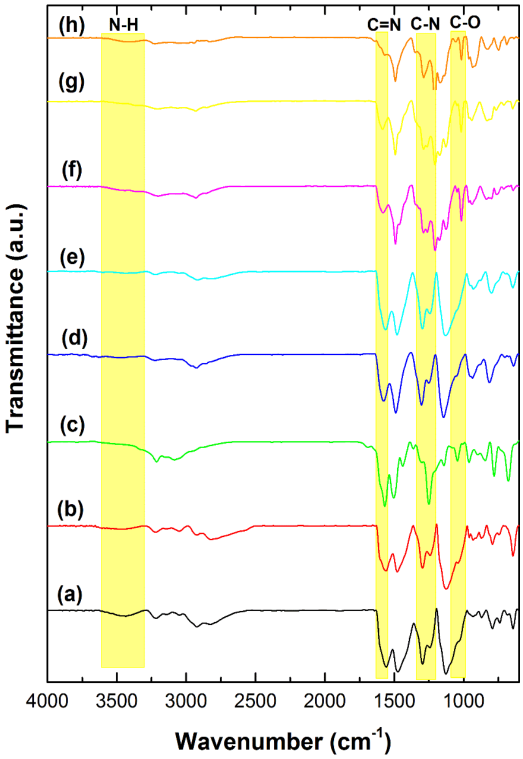

Fig. S7. FTIR spectra of (a) Polyaniline, (b) Poly(aniline-*co*-(*m*-aminophenyl boronic acid)) (3:1), (c) Poly(*m*-fluroaniline), (d) Poly (aniline-*co*-(*m*-fluoroaniline)) (1:1), (e) Poly(aniline-*co*-(*m*-fluroaniline)) (3:1), (f) Poly(*o*-methoxyaniline), (g) Poly(aniline-*co*-(*o*-methoxyaniline)) (1:1) (h) Poly(aniline-*co*-(*o*-methoxyaniline)) (3:1).

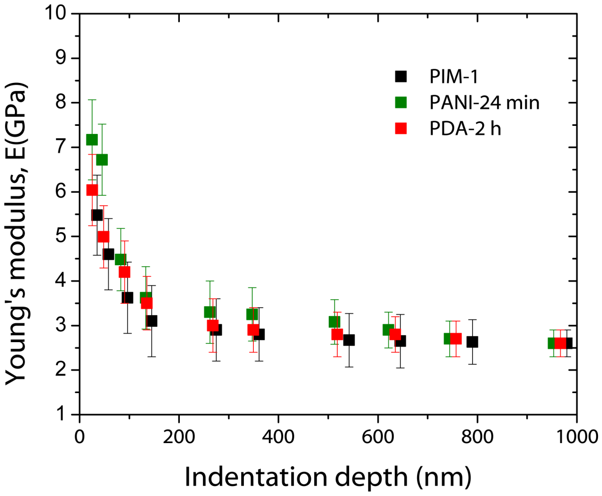

Fig. S8. Young's modulus of PIM-1, PIM-1/PDA and PIM-1/PANI membranes as a function of indentation depth.

Table S3. Pure gas permeation properties of PIM-1 and PIM-1/PDA composite membranes. All the samples prepared in dopamine concentration of 2 mg mL^{-1} and pH 8.5 (4 bar and 25 ˚C).

Reaction time (min)	Permeability (Barrer)					Selectivity				
	H_2	CO_2	O_2	N_2	CH_4	O_2/N_2	CO_2/N_2	H_2/CO_2	H_2/N_2	H_2/CH_4
0	1716	3100.7	791.8	196	210.1	4	15.8	0.6	8.8	8.2
15	1708.6	1730.9	366.5	60.6	73	6.1	28.6	1.0	28.2	23.4
30	1461.1	664	152.1	28.6	22.5	5.3	23.2	2.2	51.2	65.0
45	877.4	141.6	57.4	8.9	13.1	6.5	15.9	6.2	98.6	67.0
60	736	74.9	43.3	7.3	10.7	5.9	10.3	9.8	100.8	68.7
75	693.5	49.6	19.6	6.7	9.8	2.9	7.4	14.0	103.5	70.8
90	642.7	25.8	16.1	5.7	8.8	2.8	4.5	24.9	112.8	73.0
120	577.9	20.1	11.8	4.3	6.5	2.7	4.7	28.8	134.4	88.9
150	465.7	10.4	6.8	2.7	5.1	2.5	3.9	44.8	172.5	91.3
180	306.4	8.1	4.9	1.4	2.5	3.5	5.8	37.8	218.8	122.6

Table S4. Pure gas permeation properties of PIM-1 and PIM-1/PDA composite membranes. All the samples prepared in dopamine concentration of 4 mg mL^{-1} and pH 8.5 (4 bar and 25 ˚C).

Reaction time (min)	Permeability (Barrer)					Selectivity				
	H_2	CO_2	O_2	N_2	CH_4	O_2/N_2	CO_2/N_2	H_2/CO_2	H_2/N_2	H_2/CH_4
0	1716	3101	791.8	196.1	210.1	4	15.8	0.6	8.8	8.2
30	1675	960.7	246.7	44.1	52.6	5.9	21.7	1.7	38	31.8
60	1665	646.7	169.8	24.8	26.1	6.8	26.1	2.6	67.1	63.8
90	960.6	82.7	32.7	7.7	8.4	4.2	10.7	11.6	124.8	114.4
120	728.3	27.1	18.0	5.5	5.8	3.2	4.9	26.9	132.4	125.6

Table S5. Pure gas permeation properties of PIM-1 and PIM-1/PDA composite membranes. All the samples prepared in dopamine concentration of 1 mg mL^{-1} and pH 8.5 (4 bar and 25 ˚C).

Reaction time (min)	Permeability (Barrer)					Selectivity				
	H_2	CO_2	O_2	N_2	CH_4	O_2/N_2	CO_2/N_2	H_2/CO_2	H_2/N_2	H_2/CH_4
0	1716	3101	791.8	196.1	210.1	4	15.8	0.6	8.8	8.17
30	1245.1	438.4	125.8	30.1	23.7	4.2	14.6	2.8	41.4	52.5
60	1082.9	195.1	59.4	3.8	5.3	15.6	51.3	5.6	285	204.3
90	734.0	32.1	36.3	2.1	3.1	17.3	15.3	22.9	349.5	236.8
120	532.1	13.8	11	0.4	1.4	27.5	34.5	38.6	1330.3	380.1

Table S6. Pure gas permeation properties of PIM-1 and PIM-1/PDA composite membranes. All the samples prepared in dopamine concentration of 2 mg mL^{-1} and pH 9.5 (4 bar and 25 ˚C).

Reaction time (min)	Permeability (Barrer)					Selectivity				
	H_2	CO_2	O_2	N_2	CH_4	O_2/N_2	CO_2/N_2	H_2/CO_2	H_2/N_2	H_2/CH_4
0	1716	3101	791.8	196.1	210.1	4.0	15.8	0.6	8.8	8.2
30	1661.3	812.1	273.2	60.9	48.3	4.5	13.3	2.1	27.3	34.4
60	1205.1	245.6	76.3	12.6	21.4	6.1	19.5	4.9	95.6	56.3
90	917.70	99.60	16.6	3.4	9.1	4.9	29.3	9.2	269.9	100.9
120	829.10	36.70	14.3	2.1	7.5	6.8	17.5	22.6	394.8	110.6

Table S7. Pure gas permeation properties of PIM-1 and PIM-1/PDA composite membranes. All the samples prepared in dopamine concentration of 2 mg mL^{-1} and pH 7.5 (4 bar and 25 ˚C).

Reaction time (min)	Permeability (Barrer)					Selectivity				
	H_2	CO_2	O_2	N_2	CH_4	O_2/N_2	CO_2/N_2	H_2/CO_2	H_2/N_2	H_2/CH_4
0	1716	3101	791.8	196.1	210.1	4.0	15.8	0.6	8.8	8.2
30	1658.5	2596.3	591.8	159.4	182.3	3.7	16.3	0.6	10.4	9.1
60	1529.8	1278.3	350.2	106.8	103.9	3.3	12	1.2	14.3	14.7
90	1428.3	1002.2	231.5	39.6	50.2	5.8	25.3	1.4	36.1	28.5
120	1343.2	544.1	128.8	19.9	14.1	6.5	27.3	2.5	67.5	95.3

Table S8. Pure gas permeation properties of PIM-1 and PIM-1/PANI composite membranes (Doped with HCl) at 4 bar and 25 ˚C

Reaction time (min)	Permeability (Barrer)					Selectivity				
	H_2	CO_2	O_2	N_2	CH_4	O_2/N_2	CO_2/N_2	H_2/CO_2	H_2/N_2	H_2/CH_4
0	1716±130	3101±240.1	791.8±59.4	196.1±12.4	210.1±13.3	4±0.4	15.8±1.6	0.6±0.1	8.8±0.9	8.2±0.8
10	890.2±62.3	1601.2±110.2	312.4±25.2	90.1±5.4	99.4±5.5	3.5±0.4	17.8±1.6	0.6±0.1	9.9±0.9	9±0.8
14	598.6±48.1	1056.5±74.6	186.5±14.1	58.3±3.7	65.5±3.8	3.2±0.3	18.1±1.7	0.6±0.1	10.3±1	9.1±0.9
18	564.3±45	896.2±62.2	162.5±12.3	44.6±3.2	54.1±3.7	3.6±0.4	20.1±2	0.6±0.1	12.7±1.4	10.4±1.1
20	531.4±40.2	740.8±55.2	159.7±12	32.1±2.8	42.1±2.9	5±0.6	23.1±2.6	0.7±0.1	16.6±1.9	12.6±1.3
22	526.5±38.1	353±31.2	87.7±9.4	12.8±1.1	9.9±0.7	6.9±0.9	27.6±3.4	1.5±0.2	41.1±4.6	53.2±5.3
24	519.3±35.5	224.4±16.2	80.8±8.1	9.9±0.7	6.9±0.6	8.2±1	22.7±2.3	2.3±0.2	52.5±5.1	75.3±8.3
26	490.8±35.1	142.4±8.4	71.7±5.4	6.8±0.6	4.7±0.4	10.6±1.2	20.9±2.2	3.5±0.3	72.2±8.2	104.4±11.6
28	472.2±32.1	74.6±5.8	35.6±2.7	3.6±0.3	3.9±0.3	9.9±1.1	20.7±2.4	6.3±0.6	131.2±14.1	121±12.4
30	450.1±30.2	69.7±5.1	21.1±1.5	2.8±0.3	2.8±0.3	7.5±1	24.9±3.2	6.5±0.6	160.8±20.3	160.8±20.3
34	401.2±29.4	60.8±4.5	18.2±1.5	2.5±0.2	2.5±0.2	7.3±0.8	24.3±2.7	6.6±0.5	160.5±17.4	160.5±17.4
38	348.2±25.5	53.6±4.5	16.5±1.2	2.2±0.2	2.2±0.2	7.5±0.9	24.4±3	6.5±0.6	158.3±18.5	158.3±18.5

Table S9. Pure gas permeation properties of PIM-1/PANI copolymers composite membranes (coating times 14 and 24 min and doped in HCl) at 4 bar and 25 ˚C.

Coating layer Monomer (mol. %)	Permeability (Barrer)					Selectivity				
	H_2	CO_2	O_2	N_2	CH_4	O_2/N_2	CO_2/N_2	H_2/CO_2	H_2/N_2	H_2/CH_4
Reaction time: 14 min										
Aniline (100)	598.6	1056.5	186.5	58.3	65.5	3.2	18.1	0.6	10.3	9.1
Aniline (75) + *o*-anisidine (25)	510.4	279.8	63.8	22.9	16.0	2.8	12.2	1.8	22.3	31.8
Aniline (50) + *o*-anisidine (50)	565.7	168.8	53.8	14.5	12.0	3.7	11.7	3.4	39.0	47.1
Aniline (75) + F-aniline (25)	962.4	455.3	128.0	18.8	11.3	6.8	24.2	2.1	51.1	85.3
Aniline (50) + F-aniline (50)	1083.6	1700.1	377.3	83.5	77.2	4.5	20.4	0.6	12	14.1
Aniline (75) + APBA (25)	1349.9	1100.6	245.0	44.1	65.5	5.6	25	1.2	30.6	28.2
Reaction time: 24 min										
Aniline (100)	519.3	224.4	80.2	10	6.9	8.1	22.6	2.3	52.2	75.2
Aniline (75) + *o*-anisidine (25)	421.6	124.01	34.6	16.6	14.4	2.1	7.5	3.4	25.4	29.3
Aniline (50) + *o*-anisidine (50)	540.9	120.2	42.1	7.9	10.4	5.3	15.2	4.5	68.6	52.0
Aniline (75) + F-aniline (25)	600.9	161.3	72.8	10.2	7.3	7.2	15.8	3.7	59.0	82.7
Aniline (50) + F-aniline (50)	1065.9	547.7	151.8	25.8	15.8	5.9	21.3	2	41.4	67.6
Aniline (75) + APBA (25)	1168.4	613.9	157.7	21.5	15.6	7.4	28.6	1.9	54.5	74.9

Table S10. Effect of different doping solutions on gas permeation properties of PIM-1/PANI composite membranes (coating time 24 min) at 4 bar and 25 ˚C.

Doping solution	Permeability (Barrer)					Selectivity				
	H_2	CO_2	O_2	N_2	CH_4	O_2/N_2	CO_2/N_2	H_2/CO_2	H_2/N_2	H_2/CH_4
HCl	519.3	224.4	80.8	9.9	6.9	8.1	22.6	2.3	52.2	75.2
HBr	531	247.7	83.7	17.8	16.1	4.7	13.9	2.1	29.8	33
HI	540.7	291.2	94.0	18.1	17.3	5.2	16.1	1.9	29.8	31.3

Table S11. Physical properties of gas molecules, permeability, solubility and diffusivity of PIM-1 and PIM-1/PDA (120 min coating time) and PIM-1/PANI (24 min coating time) membranes at 25 ˚C and 4 bar.

Separation parameters	**Pure gas**					**Gas pairs**				
	H_2	**CO_2**	**O_2**	**N_2**	**CH_4**	**O_2/N_2**	**CO_2/N_2**	**H_2/CO_2**	**H_2/N_2**	**H_2/CH_4**
Critical temperature	33.2	304.2	154.6	126.3	190.9					
Kinetic diameter (Å)	2.89	3.30	3.46	3.64	3.8					
PIM-1										
P (Barrer)	1716	3101	791.9	196.10	210.1	4.04	15.81	0.55	8.75	8.17
S [10^{-3} cm^3 cm^{-3} $cmHg^{-1}$]	7.02	256.3	40.1	22.4	106.1	1.79	11.45	0.03	0.31	0.07
D (10^{-8} cm^2 s^{-1})	2446	121.0	197.6	87.6	19.8	2.26	1.38	20.21	27.92	123.54
PIM-1/PDA										
P (Barrer)	577.9	20.1	11.80	4.3	6.5	2.74	4.67	28.75	134.4	88.91
S [10^{-3} cm^3 cm^{-3} $cmHg^{-1}$]	7.9	251.3	38.1	15.9	108.3	2.39	15.78	0.03	0.49	0.07
D (10^{-8} cm^2 s^{-1})	734.5	0.8	3.10	2.7	0.6	1.15	0.30	918.13	272.0	1224.2
PIM-1/PANI										
P (Barrer)	519.3	224.4	80.8	9.9	6.9	8.16	22.67	2.31	52.45	75.26
S [10^{-3} cm^3 cm^{-3} $cmHg^{-1}$]	6.65	257.9	56.90	31.9	98.6	1.78	8.08	0.03	0.21	0.07
D (10^{-8} cm^2 s^{-1})	780.5	8.7	14.2	3.1	0.7	4.58	2.81	89.71	251.8	1115.0

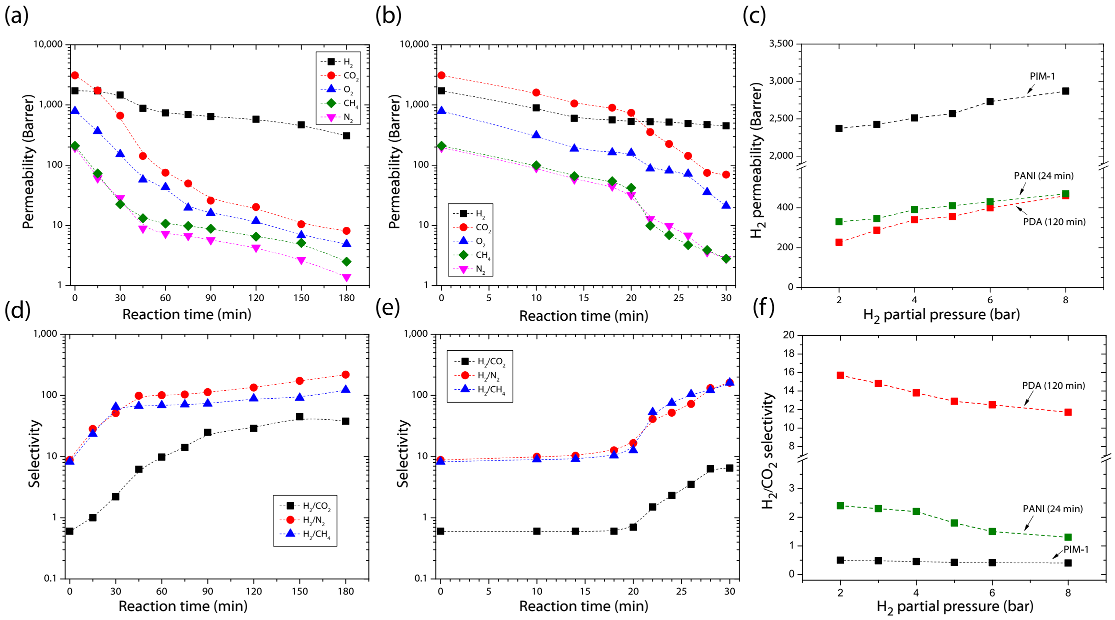

Fig. S9. (a) Single gas permeability *vs.* reaction time (2 mg mL^{-1} dopamine concentration) in PIM-1 and PIM-1/PDA composite membranes, (b) Single gas permeability *vs.* reaction time in PIM-1 and PIM-1/PANI composite membranes. (c) Mixed gas (H_2/CO_2: 50/50 vol.%) permeability of PIM-1, PIM-1/PANI (24 min reaction time) and PIM-1/PDA (120 min reaction time) composite membranes. (d) Ideal selectivity *vs.* reaction time (2 mg mL^{-1} dopamine concentration) in PIM-1 and PDA composite membranes, (e) Ideal gas selectivity *vs.* reaction time in PIM-1 and PANI composite membranes. (f) Mixed gas (H_2/CO_2: 50/50 vol.%) selectivity of PIM-1, PANI (24 min reaction time) and PDA (120 min reaction time) composite membranes.

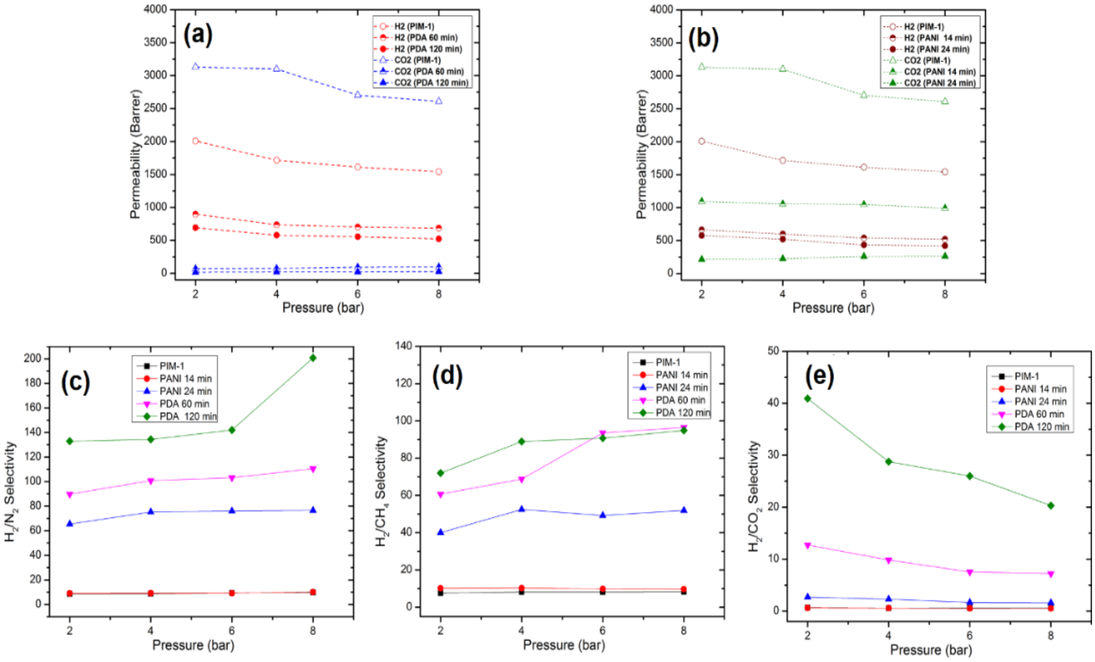

Fig. S10. Pressure dependence of gas transport properties in PIM-1/PDA and PIM-1/PANI composite membranes. (a) PIM-1/PDA single permeabilities, (b) PIM-1/PANI single permeabilities, (c) H_2/N_2, (d) H_2/CH_4 and (e) H_2/CO_2 ideal selectivities.

Structural stability of composite membranes. The structural stability of the composite membrane is an important factor from the view of practical application. Therefore, as a representative the structural stability of the PIM-1/PDA (120 min coating time, 2 mg mL^{-1} and pH 8.5) and PIM-1/PANI (24 min) composite membranes were investigated. Continuous CO_2 gas permeation tests were conducted at 4 bar and 25 ˚C. The membrane performance remains stable within the test period (Fig. S11), indicating that the PDA and PANI layers firmly adhere on the surface of PIM-1.

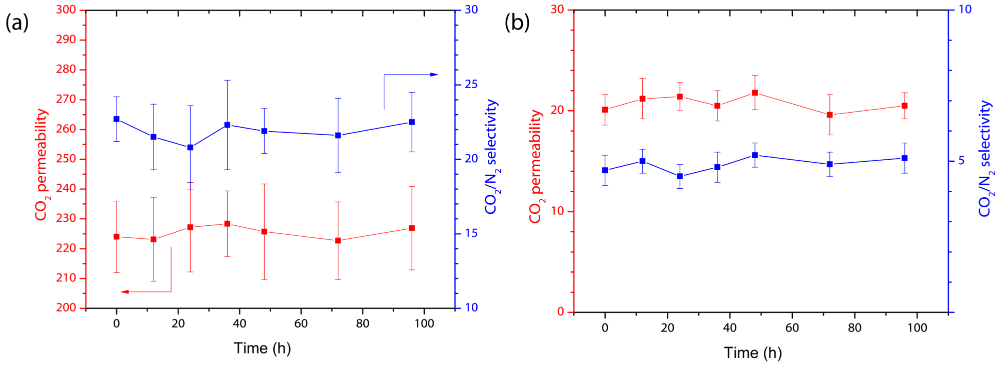

Fig. S11. Performance stability of (a) PIM-1/PDA (120 min coating time, 2 mg mL^{-1} dopamine concentration and pH 8.5) and (b) PIM-1/PANI (24 min coating time) composite membranes for up to 100 h in pure CO_2 at 4 bar and 25 ˚C.

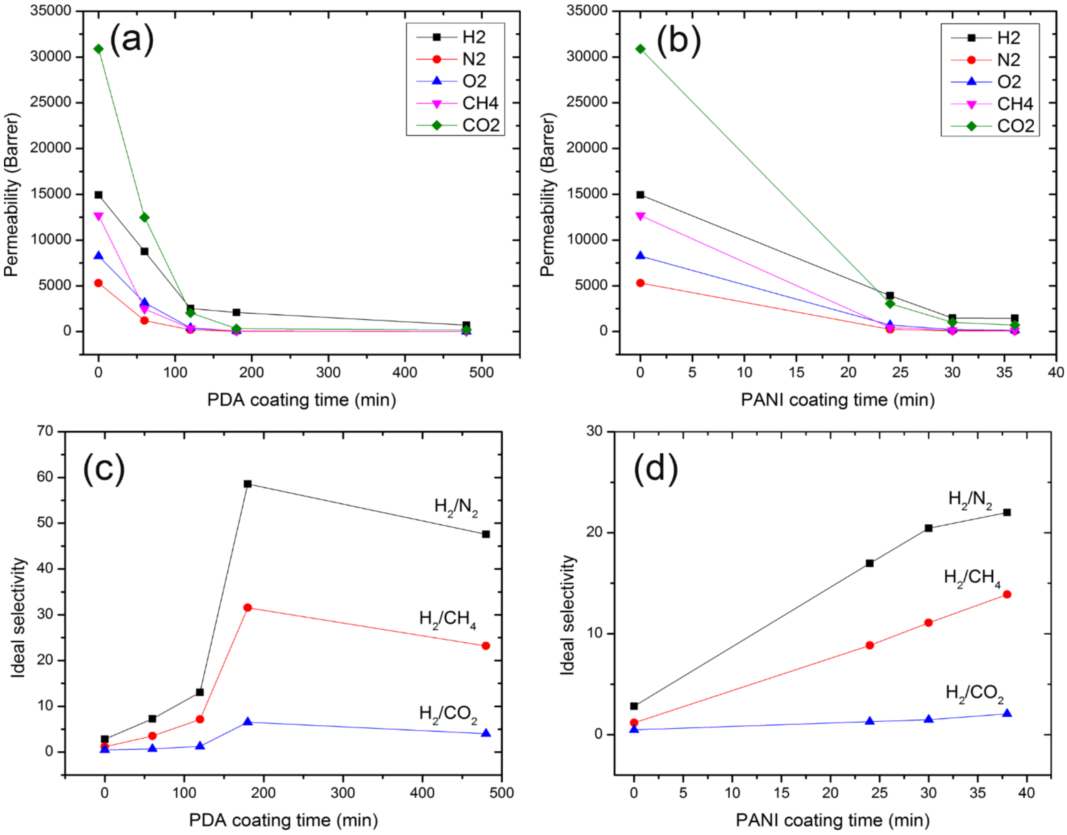

Fig. S12. Single gas permeation properties of PTMSP based composite membranes at 25 °C and 4 bar. (a) Gas permeabilities of PTMSP/PDA (b) Gas permeabilities of PTMSP/PANI (c) Ideal selectivities of PTMSP/PDA (d) Ideal selectivities of PTMSP/PANI.

Thin film composite membranes. The concept of PIM-1/PDA and PIM-1/PANI thin film membranes supported on a porous PVDF substrate was also explored in this research. Thin film of PIM-1 (thickness ~ 2 µm) have been prepared using roller blade coating machine (RK print coat instrument, UK) and 4 wt.% PIM-1 solution in chloroform on the surface of commercial PVDF ultrafiltration membrane (UF 70 KDa, AMI Co., US) (Fig. S13). In order to avoid interactions between interfacial layers and polymerization solutions, special filter holder was designed (Fig. S14). In this filter holder the polymerization solution is just in contact with the surface of PIM-1 thin film and this will decrease the growth of cracks and defects on the surface of the PIM-1 thin films. A circular piece of the PVDF support with a diameter of 10 cm was placed on stainless steel holder and sandwiched between the top stainless steel ring and the base. After assembling the holder, a defined volume of the reaction mixture solution was poured on the surface of PVDF support and was kept for completing the coating process. The separation factors of this supported, pristine PIM-1 thin film was comparable to the self-supported PIM-1 membranes (thickness around 80 µm), essentially representing a CO_2 selective membrane. By comparison, the surface polymerization of PIM-1 leads to a hydrogen selective membrane with H_2/CO_2 selectivities of 7 and 4.2 for PDA and PANI respectively at 120 and 30 min coating times (ESI, Table S12). These selectivities do not yet match those seen in the case of the 80-micron thick support and can be explained by two differences in these two (i.e. thick film and TFC) substrates. One reason is simply geometric since the self-supported PIM-1 film features surface polymerization on both sides of the polymer support whereas the PIM-1/PVDF supported membrane is coated only one side. Secondly, the thin PIM-1 layer, an essentially hydrophobic material, is prone to reorganize in the presence of a hydrophilic solvent, which can reduce the consistency for the PIM-1 support during surface polymerization. Nonetheless even the demonstrated PDA layer on PIM-1 has a selectivity which is comparable to commercial bulk polymers for hydrogen selectivity, whilst generating a hydrogen permeance of 7.1 GPU. Polyetherimide, possessing a H_2/CO_2 selectivity of 6, has H_2 permeability of 7.8 Barrer.[11] To achieve a similar permeance to that demonstrate would require a polyetherimide thin film of around 1 micron thickness. Additionally, the thickness ratio of the surface polymerized layer to the supporting PIM-1-layer thickness plays an important role, where there needs to be an optimization between the achieved selectivity and the resulting permeance of the thin film composite.

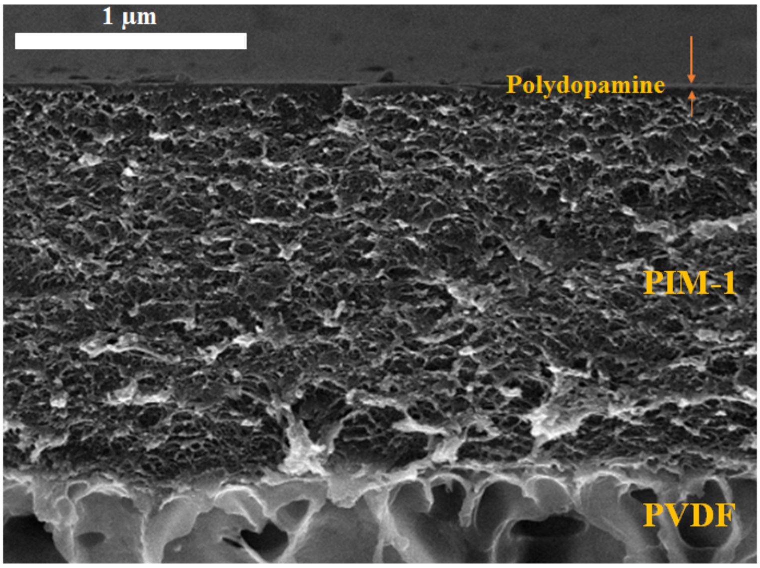

Fig. S13. Cross section SEM image of PIM-1/PDA thin film composite membranes after 120 min coating in dopamine solution (2 mg mL^{-1} and pH 8.5)

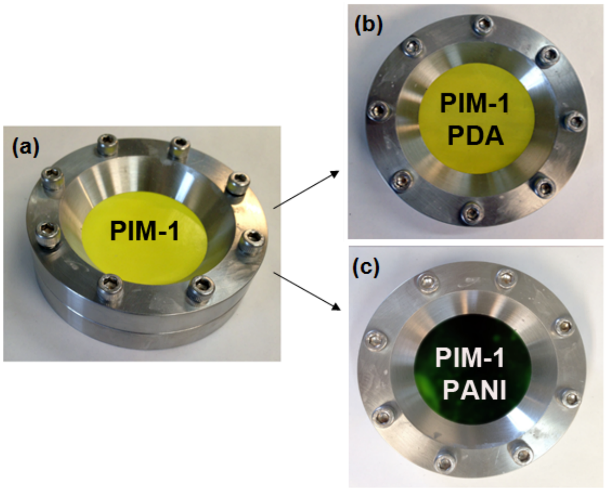

Fig. S14. Filter holder for surface polymerization of PIM-1 thin films. (a) PIM-1 thin film membrane, (b) PIM-1/PDA thin film membrane (coating time: 120 min in pH 8.5 and 2 mg mL^{-1} dopamine concentration) and (c) PIM-1/PANI thin film membrane (coating time: 24 min).

Table S12. Gas permeation of PIM-1, PIM-1/PDA (coated in dopamine concentration of 2 mg mL^{-1} and pH 8.5) and PIM-1/PANI thin film composite membranes at 4 bar and 25 ˚C.

Thin film composite membranes	Permeance (GPU)		Selectivity
	H_2	CO_2	H_2/CO_2
PIM-1	100.59	230.77	0.44
PIM-1/PDA			
120 min coating time	7.10	1.01	7.06
PIM-1/PANI			
30 min coating time	6.21	1.48	4.20

Table S13. Separation performance of representative H_2 separation polymer membranes.

Membrane	Operational conditions			Separation performance				Ref.
	Feed gas composition (H_2 vol. %)	Pressure (bar)	Temperature (K)	H_2 Permeability (Barrer)	H_2/CO_2 selectivity	H_2/N_2 Selectivity	H_2/CH_4 Selectivity	
Crosslinked PI	Pure gas	3.5	308	12	120	-	-	12
Vapor-phase crosslinked PI	Pure gas	3.5	308	125	135	-	-	13
TR-PBO	Pure gas	10	308	2.93	5.7	142	208	14
TR-poly(benzoxazole-amide)	Pure gas	20	483	1.8	8.4	199	205	14
TOX-PIM-1				1547	3	114	207	15
UV-rearranged PIM-1	Pure gas	3.5	308	452	7.3	166	173.8	16
Surface-crosslinked 6FDA-Durene-(ZIF-8)	Pure gas	3.5	308	283.5	12	141	203	17
PBI-(ZIF-7)(50)	Pure gas	3.5	308	26.2	14.9	-	-	18
PBI-(ZIF-8)(30)	50	3.5	308	105.4	12.3	-	-	19
TR-PPL	Pure gas	3	298	376	1.6	29	46	20
TR PPO-co-PI		1	303	38	3.5	95	127	21
TR PPO-co-PPL	Pure gas	3	298	1680	3.2	93	250	20

PDA and PANI thicknesses. The polydopamine and polyaniline thicknesses as a function of immersion time are presented in Figs. S15 and S16. The PDA and PANI layers were deposited on the surface of monocrystalline silicon chips and the thicknesses evaluated from the cross-sectional scanning electron microscopy. The results showed that the thickness of the layers increased with increasing the coating time. However, the layer thickness did not change linearly with time and gradually reached a constant value, e.g. 50 nm after 18 h and 140 nm after 40 min in PDA and PANI samples, respectively. Fig. S15 and S16 also show the color changes of dopamine and aniline solutions at different reaction times. The solutions turned to deep dark after 3 h and 30 min in PDA and PANI samples, respectively. As a result, the corresponding UV-visible absorption spectra of PDA and PANI solutions increased with time indicating the growth of PDA and PANI chains in the reaction solution.

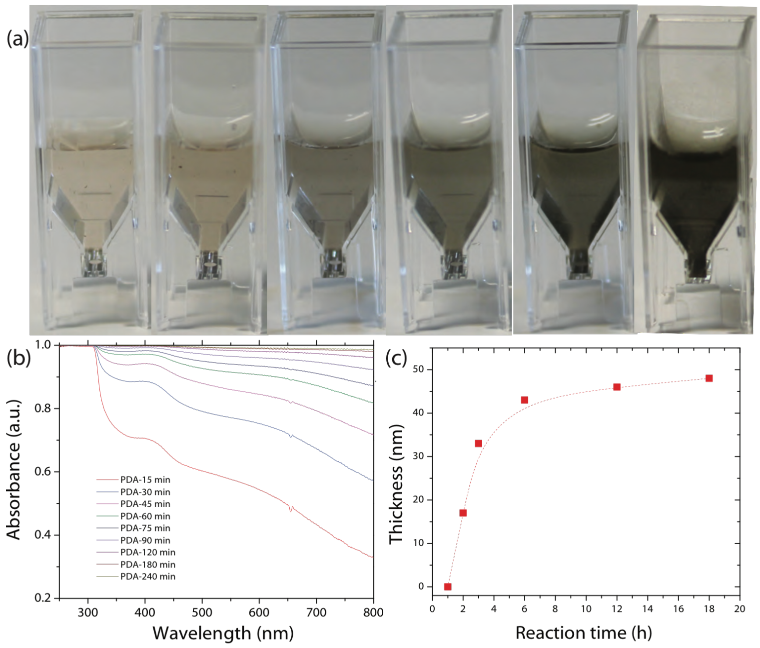

Fig. S15. (a) Color changes of dopamine solutions (2 mg mL^{-1} and pH 8.5) with time from left to right: 15, 30, 45, 60, 120 and 240 min reaction time, respectively. (b) Absorption spectral change for a dopamine solution (2 mg mL^{-1}, pH 8.5) against the reaction time. (c) SEM thickness of PDA film with respect to the polymerization time on the surface of silicon wafer.

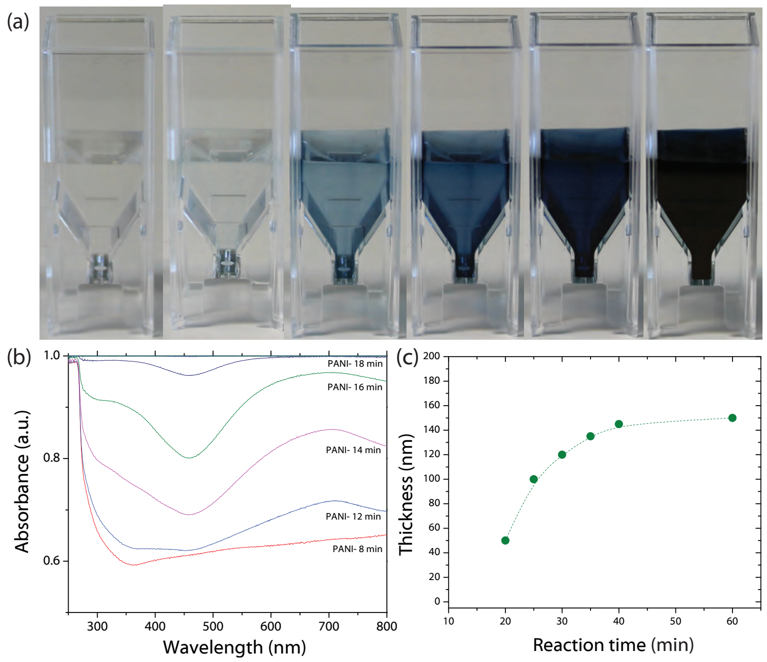

Fig. S16. (a) Color changes of polyaniline solutions with time from left to right 10, 14, 18, 22, 26 and 30 min reaction time, respectively. (b) Absorption spectral change for aniline solution against the reaction time. (c) SEM thickness of PANI film with respect to the polymerization time on the surface of silicon wafer.

Gas permeation modeling of composite membranes. The functionalization is limited to the surface region of PIM-1 and consequently coated membranes have composite structures (see SEM images, Fig. 3). In order to estimate the separation performance of the PANI and PDA layers, the resistant models (Fig. S17) is utilized.

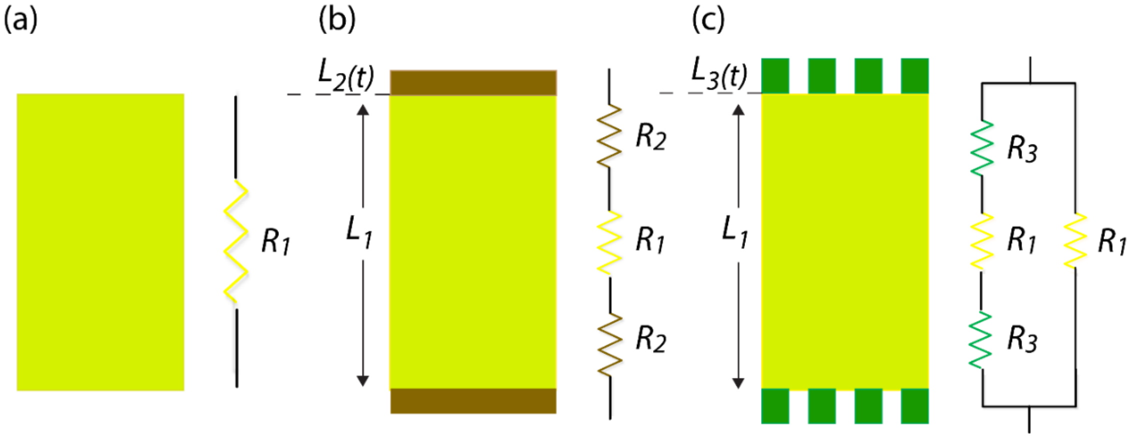

Fig. S17. Modelling of gas permeation in composite membranes. The permeability of a homogeneous PIM-1 membrane is calculated over the thickness L_1 as in (a). For asymmetric PDA and PANI functionalized PIM-1 membranes, there is a difference in the permeability and thickness of the material at the skin layer as in (b) and (c). Expressing the overall permeability as analogous to a series and parallel circuit resistance across a potential, but substituting the pressure drop for potential and resistance for permeability, the overall permeability can be determined for the changes in permeability.

Analogous to the generation of current under potential through series circuits, a resistance model can be used to describe the gas flux (*N*) under the driving force of pressure (Δ*p*) through the PDA coated membranes:

$$N = \Delta p \frac{P}{L} = \frac{\Delta p}{{L_1}/{P_1} + {2L_2(t)}/{P_2}} \tag{6}$$

Therefore, by assuming layer by layer grow of PDA on the surface of PIM-1, resistance is defined as the summation of resistance in PIM-1 and PDA layers, as following equation:

$$\left(\frac{L}{P}\right)_{cp} = \frac{L_1}{P_1} + \frac{2L_2(t)}{P_2} \tag{7}$$

Where L is the total thickness of the membrane, L_1 and P_1 are the thickness and intrinsic permeability of PIM-1 whilst P_2 and $L_2(t)$ are permeability and thickness of the PDA layer, respectively.
Furthermore, the time dependence of growth was proposed to be Arrhenius type of growth for PDA layer on the surface of PIM-1 as follow:

$$L_2(t) = a.\left(e^{-b/t}\right) \tag{8}$$

Where a and b are model parameters. The model parameters (a and b) in eq. (8) are determined by use of the least squares method (LSM) to get the best fit to the experimental permeability data. The calculated fitting parameters and intrinsic permeation properties of PDA layer in composite membranes are presented in Table S14.

Table S14. Model parameters and intrinsic permeation properties of PDA in PIM-1/PDA composite membranes

a	b	Permeability (Barrer)				
(cm)	(min)	H_2	CO_2	N_2	O_2	CH_4
2e-6	73	0.24	0.0057	0.0009	0.0035	0.0016

The oxidative polymerization and growth of PANI chains, which are insoluble in the reaction medium, proceed under heterogeneous conditions. Therefore, due to nodule like morphology of PANI layer on the surface of PIM-1, a combined resistance model, including series and parallel resistant, have been used to describe the composite resistance (*L/P*) through the PIM-1/PANI membranes:

$$\frac{1}{\left(\frac{L}{P}\right)_{cp}} = \frac{1}{\frac{L_1}{P_1}} + \frac{1}{\frac{L_1}{P_1} + \frac{2L_3(t)}{P_3}} \tag{9}$$

Where L is the total thickness of the membrane, L_1 and P_1 are the thickness and intrinsic permeability of PIM-1 whilst P_3 and $L_3(t)$ are permeability and thickness of the PANI layer, respectively.

At the beginning of coating process, we assume that PANI domains start to cover the surface of PIM-1 ($0 < t < t_1$). After the surface completely covered by PANI layer ($t > t_1$), the thickness of deposited layer would increase as an Arrhenius function of time. The estimated function for changing in PANI thickness with time is as follow:

$$L_3(t) = c.(e^{-d/t}) + L_0 \tag{10}$$

Where L_3 is the thickness of PANI layer, c and d are model parameters, t is the reaction time and L_0 is thickness of first PANI layer on the surface. In this case, both parallel resistant model ($0 < t < t_1$) and series resistant model ($t > t_1$) are applied. The model parameters in eq. (10) are calculated by use of the least squares method (*LSM*) to achieve the best fit to the experimental permeability data. The calculated fitting parameters and intrinsic permeation properties of PANI layer in composite membranes are presented in Table S15. The calculated thicknesses of PDA and PANI layers, from the modeling, in different time are presented in Fig. S18. The results here are in the same range and agreement with previous SEM thickness analysis (see Figs. S15 and S16) that showed prolonging the immersion time leads to a plateau in the coating thicknesses.

Table S15. Model parameters and intrinsic permeation properties of PANI in PIM-1/PANI composite membranes.

c	d	t_1	L_0	Permeability (Barrer)				
(cm)	(min)	(min)	(cm)	H_2	CO_2	N_2	O_2	CH_4
1.5e-5	9	22	2.7e-6	0.6	0.15	0.0064	0.05	0.0058

Table S16. Permeabilities and ideal separation factors for polyaniline membranes reported in the literature.

Permeability (Barrer)					Selectivity				
H_2	N_2	O_2	CH_4	CO_2	H_2/CO_2	H_2/N_2	CO_2/N_2	O_2/N_2	Ref.
1.41	0.0001	0.07	-	0.156	7.3	207	28.3	9.5	22
4.38	0.0165	0.151	0.0078	0.72	6.1	265	38.7	9.1	23
4.35	0.01	0.142		0.55	7.9	435	55	14.2	24
1.5	0.009	0.088		0.29	5.2	166.7	32.2	9.8	25
3.33	0.022	0.11	-	0.64	9	150.8	16.8	4.9	26
-	-	-	-	-	8.6	348	40.4	7.1	27

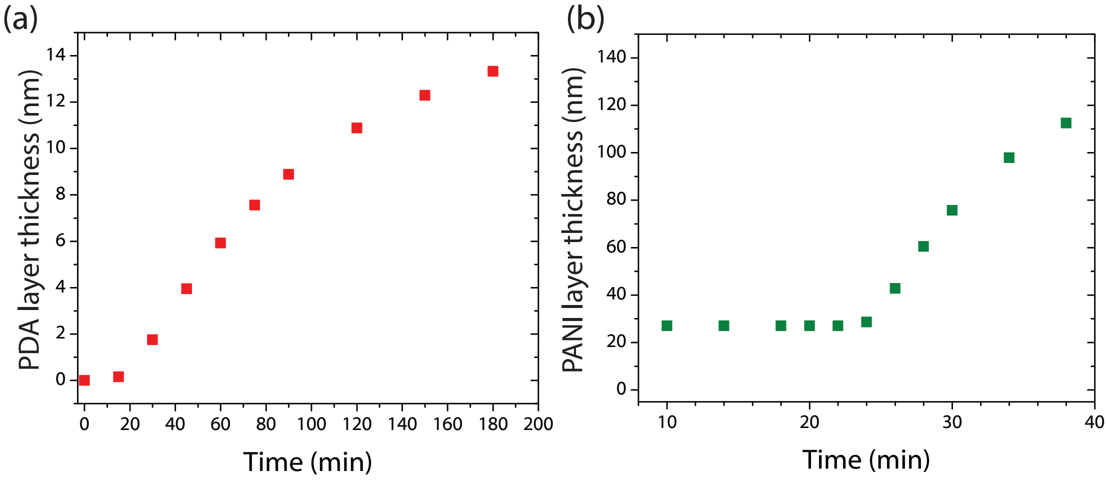

Fig. S18. Calculated coating layer thicknesses *vs.* time from modeling data (a) Polydopamine and (b) Polyaniline.

References:

1. P. M. Budd, E. S. Elabas, B. S. Ghanem, S. Makhseed, N. B. McKeown, K. J. Msayib, C. E. Tattershall and D. Wang, *Advanced Materials*, 2004, **16**, 456-459.
2. W. C. Oliver and G. M. Pharr, *Journal of materials research*, 1992, **7**, 1564-1583.
3. B. Li, W. Liu, Z. Jiang, X. Dong, B. Wang and Y. Zhong, *Langmuir*, 2009, **25**, 7368-7374.
4. Z.-Y. Xi, Y.-Y. Xu, L.-P. Zhu, Y. Wang and B.-K. Zhu, *Journal of Membrane Science*, 2009, **327**, 244-253.
5. P. Mokreva, D. Tsocheva, G. Ivanova and L. Terlemezyan, *Journal of applied polymer science*, 2006, **99**, 75-81.
6. A. L. Sharma, V. Saxena, S. Annapoorni and B. Malhotra, *Journal of applied polymer science*, 2001, **81**, 1460-1466.
7. R. A. Zangmeister, T. A. Morris and M. J. Tarlov, *Langmuir*, 2013, **29**, 8619-8628.
8. L. Zhang, J. Shi, Z. Jiang, Y. Jiang, S. Qiao, J. Li, R. Wang, R. Meng, Y. Zhu and Y. Zheng, *Green Chemistry*, 2011, **13**, 300-306.
9. N. V. Blinova and F. Svec, *Journal of Membrane Science*, 2012, **423**, 514-521.
10. A. Y. Arasi, J. J. L. Jeyakumari, B. Sundaresan, V. Dhanalakshmi and R. Anbarasan, *Spectrochimica Acta Part A: Molecular and Biomolecular Spectroscopy*, 2009, **74**, 1229-1234.
11. V. Abetz, T. Brinkmann, M. Dijkstra, K. Ebert, D. Fritsch, K. Ohlrogge, D. Paul, K. V. Peinemann, S. Pereira-Nunes and N. Scharnagl, *Advanced Engineering Materials*, 2006, **8**, 328-358.
12. B. T. Low, Y. Xiao and T. S. Chung, *Polymer*, 2009, **50**, 3250-3258.
13. H. Wang, D. R. Paul and T.-S. Chung, *Journal of Membrane Science*, 2013, **430**, 223-233.
14. Y. S. Do, J. G. Seong, S. Kim, J. G. Lee and Y. M. Lee, *Journal of Membrane Science*, 2013, **446**, 294-302.
15. Q. Song, S. Cao, R. H. Pritchard, B. Ghalei, S. A. Al-Muhtaseb, E. M. Terentjev, A. K. Cheetham and E. Sivaniah, *Nature communications*, 2014, **5**.
16. F. Y. Li, Y. Xiao, Y. K. Ong and T. S. Chung, *Advanced Energy Materials*, 2012, **2**, 1456-1466.
17. S. N. Wijenayake, N. P. Panapitiya, S. H. Versteeg, C. N. Nguyen, S. Goel, K. J. Balkus Jr, I. H. Musselman and J. P. Ferraris, *Industrial & Engineering Chemistry Research*, 2013, **52**, 6991-7001.
18. T. Yang, Y. Xiao and T.-S. Chung, *Energy & Environmental Science*, 2011, **4**, 4171-4180.
19. T. Yang, G. M. Shi and T. S. Chung, *Advanced Energy Materials*, 2012, **2**, 1358-1367.
20. J. I. Choi, C. H. Jung, S. H. Han, H. B. Park and Y. M. Lee, *Journal of Membrane Science*, 2010, **349**, 358-368.
21. C. H. Jung, J. E. Lee, S. H. Han, H. B. Park and Y. M. Lee, *Journal of Membrane Science*, 2010, **350**, 301-309.
22. M. R. Anderson, B. R. Mattes, H. Reiss and R. B. Kaner, *Science*, 1991, **252**, 1412-1415.
23. H. Wang and B. Mattes, *Synthetic metals*, 1999, **102**, 1333-1334.

24. L. Rebattet, M. Escoubes, E. Genies and M. Pineri, *Journal of applied polymer science*, 1995, **57**, 1595-1604.
25. G. Illing, K. Hellgardt, M. Schonert, R. Wakeman and A. Jungbauer, *Journal of membrane science*, 2005, **253**, 199-208.
26. G. Illing, K. Hellgardt, R. Wakeman and A. Jungbauer, *Journal of Membrane Science*, 2001, **184**, 69-78.
27. Y. Gupta, K. Hellgardt and R. Wakeman, *Journal of membrane science*, 2006, **282**, 60-70.